Quartz tuning forks with novel geometries for optoacoustic gas sensing

V. Spagnolo[a*], A. Sampaolo[a,b], P. Patimisco[a,b], L. Dong[b], Y. Gupta[b], Y. Yu[b], A. Geras[b,c], M. Giglio[a], P.P. Calabrese[a], T. Starecki[c], G. Scamarcio[a], and Frank K. Tittel[b]

[a]Dipartimento Interateneo di Fisica, University and Politecnico of Bari, CNR-IFN UOS BARI, Via Amendola 173, Bari, Italy; [b] Department of Electrical and Computer Engineering, Rice University, 6100 Main Street, Houston, TX 77005, USA; [c]Institute of Electronic Systems, Warsaw University of Technology, Nowowiejska 15/19, 00-665 Warsaw, Poland

ABSTRACT

We report the successful realization of quartz-enhanced photo-acoustic (QEPAS) sensors employing quartz tuning forks (QTFs) with novel geometrical parameters. We investigated the influence of QTF sizes on the main resonator parameters, in order to identify the best design parameters optimizing the QTF figures of merit for optoacoustic gas sensing. To evaluate the QTF acousto-electric energy conversion efficiency, we operated the QEPAS sensors in the near-IR and selected water vapor as the target gas. QTFs are forced to resonate at both the fundamental and the first overtone vibrational mode frequencies. Our results shows that two QTF designs exhibit an higher quality factor (and consequently an higher QEPAS signal) when operating on the first overtone mode with respect to the fundamental one.

Keywords: Quartz tuning fork, Quartz Enhanced Photoacoustic Spectroscopy, Gas Sensing

1. INTRODUCTION

Quartz crystal tuning forks (QTFs) are central components for timing and frequency measurements, thanks to their high stability, precision, and low power consumption. They are mass-produced and represent the most commonly used electronic component when a stable frequency reference is required such as clocks, smartphones and digital electronics. Being time measurements the main application, QTFs crystal cut, size and geometry have been optimized only to keep a selected resonance frequency (typically 2^{15}~ 32.7 KHz) in a wide temperature range around room temperature. However, recently, the use of QTFs has been extended to sensing applications, such as atomic force microscopy (AFM) [1-3] and near-field optical microscopy [4]; optoacoustic gas sensing [5,6]; viscosimetry [7]; accelerometers and gyroscopes [8].

All these applications rely on an enhancement of different QTF parameters: the resonator quality factor, the resonance frequency, the fork stiffness and the spring constant). Thus, studies of the dependence of resonator parameters as a function of QTF sizes are required to identify the optimal QTF design enhancing its sensing performances.

Among the different sensing techniques employing QTF as piezoelectric transducer, Quartz-Enhanced Photo-Acoustic Spectroscopy (QEPAS) allows to detect extremely low gas concentrations, down to few parts per trillion in volume [9-10]. This method employs a QTF as piezoelectric transducer to convert weak sound waves, produced by the gas target light absorption, into an electrical signal. QTFs designed as frequency standard at 32.8 kHz in clocks and smartphones have been usually employed in QEPAS sensors. Since the prong spacing is ~ 300 μm, the main difficulty is the proper focalization of the laser beam between the prongs without hitting them. Moreover, as already mentioned, no optimization of the QTF size and geometry was pursued for trace gas sensing applications.

With this aim, we realized several QTFs with different geometries by varying prong lengths and thicknesses, to reduce the QTF resonant frequency to a few kHz, and selecting larger prongs spacings (400-800 μm), in order to facilitate the laser beam focusing between the QTF prongs [11]. A detailed investigation of the influence of the QTF sizes on the main physical parameters, namely, the quality factor Q, the resonance frequency, the fork stiffness, the spring constant, and the electrical resistance is presented. Custom QTFs were mounted in a QEPAS assembly and tested in the near-IR range by using a diode laser operating at 1.37 μm. The QEPAS sensor has been tested by detecting water vapor as the target gas and operate the QTFs at the first and, when possible, at the first overtone mode. Depending on the QTFs design, the first overtone resonance can provide QEPAS signal-to-noise ratio greater with respect to that measured for the fundamental mode [12].

Quantum Sensing and Nano Electronics and Photonics XIII, edited by Manijeh Razeghi, Gail J. Brown, Jay S. Lewis, Proc. of SPIE Vol. 9755, 97552L · © 2016 SPIE
CCC code: 0277-786X/16/$18 · doi: 10.1117/12.2209530

2. QUARTZ TUNING FORKS THEORETICAL MODEL

QTF is an acoustic resonator in the form of a two-pronged fork with the prongs (tines) connected at one end. The resonance frequencies are defined by the elastic properties (Young modulus) of the quartz material, from which it is made, and by its geometry. The symmetry of the two prongs reduces the number of possible modes with a good quality factor. Being quartz a piezoelectric material, the mechanical excitation of the QTF can be converted in an electrical excitation and vice versa. To verify that a QTF crystal behaves like an electro-optic transducer, it must be calibrated in terms of resonance frequency, resonance width and oscillator's amplitude. Each single prong can be described using a single oscillator model, neglecting the coupling with the other prong. Moreover, under small amplitude oscillations, the motion of each tine can be simplified to a one-dimensional model. With a sinusoidal excitation, the equation of motion for the top of the prong in the vacuum is given by:

$$m_e \frac{d^2x}{dt^2} + m_e\beta\frac{dx}{dt} + kx = F_0\cos(\omega t + \delta) \tag{1}$$

where F_0 is the driving force of the tuning fork at an angular frequency ω, x is the displacement of the prong top perpendicularly to the tine axis, m_e is the effective mass of one prong, β is the damping coefficient for unit mass, and k is the spring constant of the prong. The effective mass of one prong is given in vacuum by $m_e = 0.24267\rho LTw$ [4], where ρ = 2650 kg/m^3 is the density of quartz, and the sizes L, T and w are shown in Fig. 1.

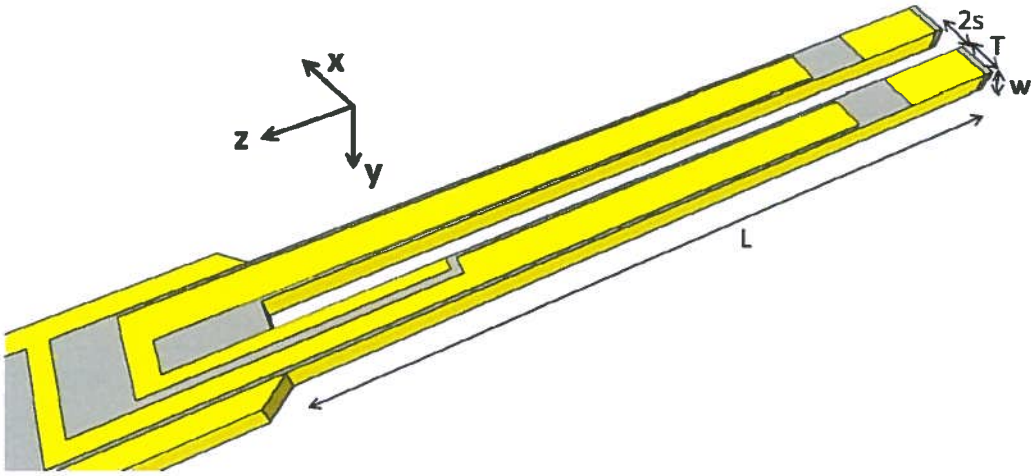

Figure 1. Schematic view of dimensions of a quartz tuning fork and its coordinate system.

The frequencies of the vibration modes of a single beam are obtained by solving the classical Euler-Bernoulli equation, [11].

$$EI_{in}\frac{\partial^4 x}{\partial z^4}(z,t) + \rho A\frac{\partial^4 x}{\partial t^4}(z,t) = 0 \tag{2}$$

where E = 72 GPa is the quartz Young's modulus, I_{in} is the moment of inertia of the prong, and $A = T \cdot w$ is the cross sectional area. By solving Eq. (2) and including clamped-free boundary condition, one can calculate the resonance frequencies in vacuum by using the following equation:

$$f_{n,vac} = \frac{\pi T}{8\sqrt{12}L^2}\sqrt{\frac{E}{\rho}}n^2 \tag{3}$$

where n = 1.194 for the lowest flexural mode of oscillation (fundamental mode) and n = 2.988 for the first overtone mode [13]. In the fundamental mode, each prong vibrates with an antinode at the tip and a node at the base. Assuming that each prong is described as a single harmonic oscillator, the fundamental frequency f_0 can be also expressed by:

$$f_0 = \frac{\omega_0}{2\pi} = \frac{1}{2\pi}\sqrt{\frac{k_0}{m_e}} \tag{4}$$

The spring constant (or stiffness) k_0 of the fundamental mode of a prong is determined straightforwardly from its geometrical parameters and elastic properties and it reads:

$$k_0 = 0.2575\frac{Tw^3E}{L^3} \tag{5}$$

It is convenient to introduce the quality factor Q defined as the ratio of f_0 to the full width at half-maximum (FWHM) value of the resonance curve Δf. In the approximation of harmonic oscillator, $Q = f_0/\beta$, i.e. $\beta = \Delta f$.

Due to the quartz piezoelectric effect, these oscillations of the tines create charges and cause a current that is proportional to the velocity of the top of the tine: $I(t) = adx/dt$, where a is the so-called fork constant. Its theoretical value is given by:

$$a = 3d_{11}E\frac{Tw}{L} \tag{6}$$

where $d_{11} = 2.31\cdot10^{-12}$ m/V or C/N is the longitudinal piezoelectric modulus of quartz [14]. Thus, the QTF can be treated both as a mechanical oscillator and as an RLC circuit. The electrical equivalent equation to that of motion, in the absence of parasitic capacitances in the circuit, is:

$$\frac{d^2I}{dt^2} + \frac{R}{L}\frac{dI}{dt} + \frac{I}{LC} = \frac{1}{L}\frac{dV(t)}{dt} \tag{7}$$

where $V(t)$ is a sinusoidal driving voltage, I is the QTF current, R its resistance, L its inductance, and C its capacitance. Using Eq. (1), Eq. (6) and Eq. (7), we may relate the mechanical and electric behaviour of the QTF: $R = 2m_e\beta/a^2$, $L = 2m_e/a^2$ and $C = a^2/2k$. We can then restate the fork constant as:

$$a = \sqrt{\frac{2m_e\beta}{R}} = \sqrt{\frac{2m_e\Delta f}{R}} \tag{8}$$

The solution for Eq. (7) can be written as $I(t) = I_a sin(2\pi ft) + I_d cos(2\pi ft)$, where I_a and I_d are the current in-phase and out-of-phase components, respectively, and are both functions of the driving frequency f:

$$I_a = \frac{I_M(\Delta f)^2 f^2}{(\Delta f)^2 f^2 + \left(f^2 - f_{0,vac}^2\right)^2},\quad I_b = \frac{fI_M\Delta f\left(f^2 - f_{0,vac}^2\right)}{(\Delta f)^2 f^2 + \left(f^2 - f_{0,vac}^2\right)^2} \tag{9}$$

where I_M is the maximum current value at the resonant frequency $f_{0,vac}$ [15].

3. QTF DESIGN

Starting from z-cut quartz wafer with 2-degree rotation along x-axis, standard photolithographic techniques were used to etch the QTF. The QTFs crystal pattern is transferred from photomask into wafer by photolithographic technique, three-dimension crystal is generated by chemical etching in hydrogen fluoride solution and finally side electrodes

(450Å/2500Å Chromium/gold layer) are applied through shadow masks. In Table 1 are reported the main geometrical parameters for the investigated QTFs.

TABLE 1. Dimensions and prong effective mass me of the standard and custom tuning forks: L (QTF prong length), T (thickness of the prong), w (thickness of the quartz crystal) and 2s (spacing between prongs).

Dimension (mm)	QTF #1	QTF #2	QTF #3	QTF #4
L	3.5	10.0	11.0	17.0
w	0.25	0.25	0.25	0.25
T	0.2	0.9	0.5	1.0
Prong spacing 2s	0.4	0.8	0.6	0.7

Being stability and accuracy needed to study QTFs because of their typically high quality factors, the experimental setup used in this work is schematically depicted in Fig. 2.

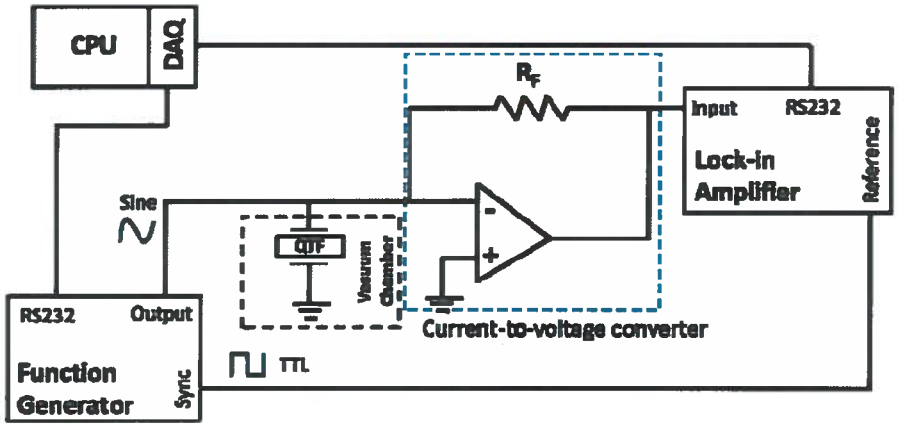

Figure 2. Schematic of the apparatus used for the QTF electrical characterization. RF: feedback. DAQ: Data Acquisition Card.

A Tektronix model AFG3102 function generator with a resolution and accuracy of 2 mHz was used to provide a sinusoidal voltage to the samples. The QTFs current passes through a current to voltage converter using an operational amplifier. The voltage at the output of the current-voltage converter is measured by a lock-in amplifier. The lock-in detection allowed us to detect low amplitude signals in a noisy environment and to separately measure the absorption (I_a) and dispersion (I_d) components of the current, synchronized with the frequency of the function generator. To determine the resonance properties of the QTFs, we slowly varied the frequency of the function generator and processed the lock-in output via a data acquisition (DAQ) card and a computer (CPU). The frequency responses of the investigated QTFs, obtained at a pressure of 50 Torr in standard air and with an excitation voltage level of V_0 = 0.5 mV, for both the fundamental and first overtone flexural modes are shown in Fig. 3.

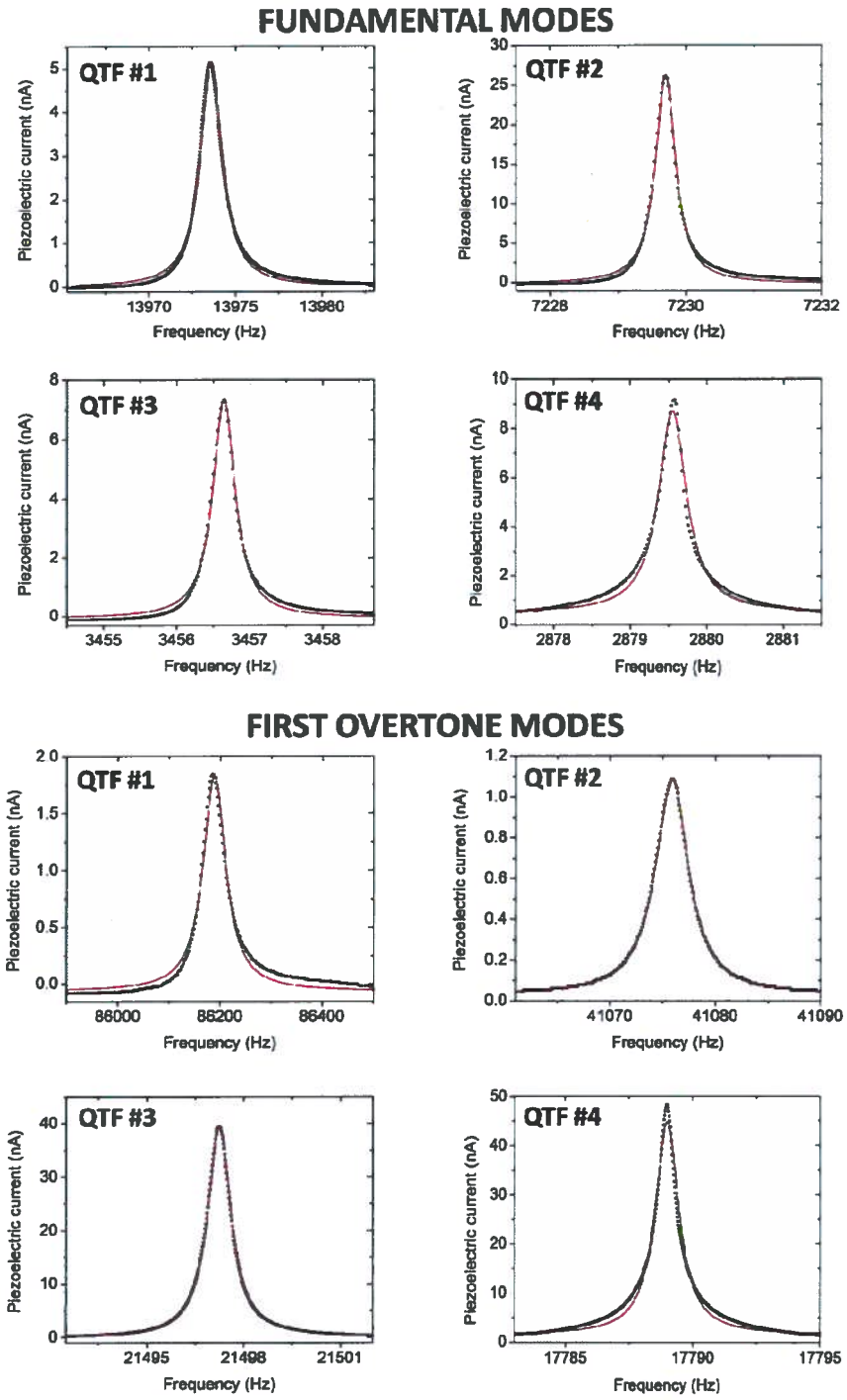

Figure 3. In-phase current I_a (black symbols) components measured for the first overtone mode of QTF#1, QTF#2, QTF#3 and QTF#4 as a function of the exciting frequency, at a voltage level $V_0 = 0.5$ mV, in standard air and atmospheric pressure. The red curves are the best fits obtained using the first of Eqs. (9).

From the resonance curves we can extract the resonance frequency of the fundamental flexural mode $f_0^{(meas)}$, the current amplitude I_M at the resonant frequency, the quality factor Q and the spring constants (k_n) by using Eq. (4). For the first overtone mode, the effective dynamic spring constant results:

$$k_1 = k_0\left(\frac{1.194}{2.988}\right)^2 \tag{10}$$

From the resonance characteristics measured as a function of the excitation voltage amplitude V_0, it is possible to determine the electrical resistance $R = V_0/I_M$, since at resonance the QTF behaves like a pure omhnic resistor. In Table II we reported the obtained experimental data together with the corresponding theoretical resonant frequencies $f_{0,vac}$ calculated under vacuum condition by using Eq. (3).

TABLE II. Measured $f_n^{(meas)}$ (resonance frequency), Q_n (quality factor), I_M (current amplitude at the resonance frequency), k_n (spring constant) and resistance for QTF#1, 2, 3, 4, for the fundamental (n = 0) and first overtone (n = 1) mode. Theoretical resonant frequencies $f_n^{(theo)}$ are also listed.

	QTF#1		QTF#2	
	fundamental n = 0	**1st overtone n = 1**	**fundamental n = 0**	**1st overtone n = 1**
$f_n^{(meas)}$ (Hz)	13973.47	86182.09	7229.68	41075.90
$f_n^{(theo)}$ (Hz)	13746.59	86088.96	7577.81	47456.54
Q_n	9144.94	1649.61	20256.87	10770.33
R_n (kΩ)	675.08	1870.29	131.74	3195.53
I_M (nA)	5.13	1.85	26.30	1.08
k_n (N/m)	866.73	138.40	2983.02	476.32
	QTF#3		**QTF#4**	
	fundamental n = 0	**1st overtone n = 1**	**fundamental n = 0**	**1st overtone n = 1**
$f_n^{(meas)}$ (Hz)	3456.62	21497.23	2879.55	17788.95
$f_n^{(theo)}$ (Hz)	3479.25	21789.04	2913.42	18245.50
Q_n	9202.93	24533.77	12098.97	31373.81
R_n (kΩ)	471.29	87.85	373.50	70.40
I_M (nA)	7.35	39.47	9.28	49.22
k_n (N/m)	416.72	66.54	893.55	142.68

A very good agreement between experimental and theoretical f_n values was obtained. The small discrepancies are mostly due to a damping gas effect, additional weight of the electrode gold layers, and slight deviations in the geometry between the modeled and the real QTFs [13]. The data in Table II show that for QTF#3 and QTF#4, the first overtone mode is characterized by higher Q-factor and peak current signal, with respect to the fundamental mode. High Q-factors and electrical conductances provide a high QEPAS signal [13, 16], which implies that operating with first overtone flexural mode could offer an improved performance in terms of trace gas sensing applications for QTF#3 and #4. However, resonance frequencies higher than 32 KHz even for a fast relaxing gas such as water vapor do not allow an efficient vibrational-translational energy transfer and the corresponding QEPAS signal results very small. Thus, we were able to perform QEPAS experiment using the first overtone mode only for QTF#3and #4. We implemented the custom QTF in the QEPAS setup and selected water vapor as the target gas. The selected water line falls at 7299.43 cm^{-1} and has a line-strength of 1.01×10^{-20} cm/mol, according to the Hitran database [17]. A diode laser emitting at 1.37 μm was used as exciting source. The laser beam was focused between the prongs of the QTF by using a lens with a focal length of 40 mm. The acoustic detection module containing the QTF was filled with air samples with a concentration of 1.7 % of

water. In a first step, we optimized the QEPAS detection performance in terms of signal-to-noise ratio by appropriately select the gas pressure the wavelength modulation depth and the diode laser beam positions between the QTF prongs. For both QTF#3 and #4 at the optimum operating conditions, the largest QEPAS signal was observed for the first overtone mode. The spectral scans obtained for QTF#3 at each vibrational mode are shown in Fig. 4.

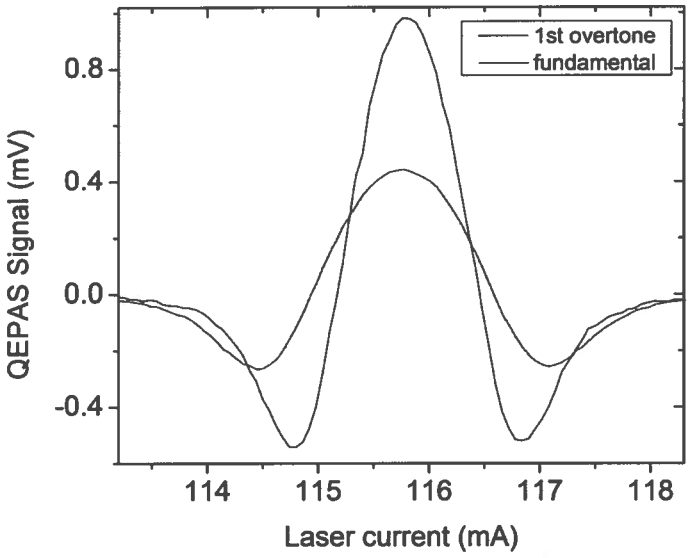

Figure 4. QEP AS spectral scans of a gas mixture containing air with a 1.7% water concentration at a pressure of 75 Torr for the fundamental mode (black solid line) and the first overtone one (red solid line), acquired at the optimum laser modulation depth and focusing point conditions. Both scans were recorded with a 100 ms lock-in integration.

These results clearly demonstrate that for the investigated QTF#3 and #4 operating in the first overtone flexural mode is advantageous in terms of QEPAS signal-to-noise ratio. These results open the way to employing QTF overtone vibrational modes for QEPAS based trace gas sensing.

REFERENCES

[1] Atia W. A. and Davis C. C., "A phase-locked shear-force microscope for distance regulation in near-field optical microscopy," Appl. Phys. Lett. 70, 405 (1997).

[2] Edwards H., Taylor L., Duncan W. and Melmed A. J., "Fast, high-resolution atomic force microscopy using a quartz tuning fork as actuator and sensor," J. Appl. Phys. 82, 980 (1997).

[3] Schmidt J. U., Bergander H. and Eng L. M., "Shear force interaction in the viscous damping regime studied at 100 pN force resolution," J. Appl. Phys. 87, 3108 (2000).

[4] Karrai K. and Grober R. D., "Piezoelectric tip-sample distance control for near field optical microscopes," Appl. Phys. Lett. 66, 1842 (1995).

[5] Patimisco P., Scamarcio G., Tittel F. K. and Spagnolo V., "Quartz-Enhanced Photoacoustic Spectroscopy: A Review," Sensors 14, 6165 (2014).

[6] Kosterev A. A., Tittel F. K., Serebryakov D., Malinovsky A. and Morozov A., "Applications of quartz tuning forks in spectroscopic gas sensing," Rev. Sci. Instrum. 76, 043105 (2005).

[7] Garg D., Efimov V. B., Giltrow M., McClintock P. V. E., Skrbek L. and Vinen W. F., "Behavior of quartz forks oscillating in isotopically pure 4He in the $T \rightarrow 0$ limit," Phys. Rev. B 85, 144518 (2012).

[8] Kudo S., "Consideration on Temperature Characteristics of Sensitivity in Quartz Tuning Fork Gyroscope," Jpn. J. Appl. Phys. 37, 2872 (1998).

[9] Spagnolo V., Patimisco P., Borri S., Scamarcio G., Bernacki B. E. and Kriesel J., "Part-per-trillion level detection of SF_6 using a single-mode fiber-coupled quantum cascade laser and a quartz enhanced photoacoustic sensor," Opt. Lett. 37, 4461 (2012).
[10] Spagnolo V., Patimisco P., Borri S., Scamarcio G., Bernacki B.E., Kriesel J., "Mid-infrared fiber-coupled QCL-QEPAS sensor," Appl. Phys. B 112, 25–33 (2013).
[11] Patimisco P., Sampaolo A., Dong L., Giglio M., Scamarcio G., Tittel F. K. and Spagnolo V., "Analysis of the electro-elastic properties of custom quartz tuning forks for optoacoustic gas sensing," submitted to Sensors Actuat. B-Chem (2015)
[12] Sampaolo A., Patimisco P., Dong L., Geras A., Scamarcio G., Starecki T., Tittel F. K. and Spagnolo V., "Quartz-enhanced photoacoustic spectroscopy exploiting tuning fork overtone modes," Appl. Phys. Lett. 107, in press (2015)
[13] Patimisco P., Borri S., Sampaolo A., Beere H. E., Ritchie D. A., Vitiello M. S., Scamarcio G. and Spagnolo V., "A quartz enhanced photo-acoustic gas sensor based on a custom tuning fork and a terahertz quantum cascade laser,"Analyst 139, 2079 (2014).
[14] Giessibl F. J., Pielmeier F., Eguchi T., An T. and Hasegawa Y., "Comparison of force sensors for atomic force microscopy based on quartz tuning forks and length-extensional resonators," Phys. Rev. B 84, 125409 (2011).
[15] Bradley D. I., Fear M. J., Fisher S. N., Guénault A. M., Haley R. P., Lawson C. R., Pickett G. R., Schanen R., Tsepelin V. and Wheatland L. A., "Stability of flow and the transition to turbulence around a quartz tuning fork in superfluid 4He at very low temperatures," Phys. Rev. B 89, 214503 (2014).
[16] Kosterev A. A., Bakhirkin Y. A., and Tittel F. K., "Ultrasensitive gas detection by quartz-enhanced photoacoustic spectroscopy in the fundamental molecular absorption bands region," Appl. Phys. B 80, 133 (2005).
[17] Rothman L. S., et al., "The HITRAN 2013 molecular spectroscopic database," J. Quant. Spectros. Radiat. Transfer 130, 4 (2013).